SLAC–PUB–8035

December, 1998

# SPIN-POLARIZED ELECTRONS: GENERATION AND APPLICATIONS*

A. V. Subashiev†, Yu. A. Mamaev, and Yu. P. Yashin

*Technical University, St.Petersburg, 195251, Russia*

J. E. Clendenin

*Stanford Linear Accelerator Center, Stanford, CA 94309, USA*

## Abstract

Current progress in experimental and theoretical investigations of polarized electron emission from semiconductor heterostructures as well as in the development of photoemitters of highly polarized electrons is reviewed. Special attention is paid to the problems of the optimal choice of the photocathode structure, kinetics in the band bending region, and emission current and charge limitations in the case of intense optical pumping. Examples of the application of highly-polarized electron sources in medium- and high-energy physics and in the investigation of surface magnetism are discussed.

*To be published in volume 1/2 (1999), of the international journal*

*Physics of Low-Dimensional Structures*

*in honor of the late V.A. Grazhulis, Professor of Physics*

*Institute of Solid State Physics, Russian Academy of Sciences*

---

*Work supported by the Russian State Program "Surface atomic structures" project 95-1.23, by the U.S. Civilian Research and Development Foundation award RP1-351, by the Russian Foundation for Basic Research project 96-02-19187, and by the U.S. Department of Energy contract DE-AC03-76SF00515.

†e-mail: arsen@subashiev.hop.stu.neva.ru

**Contents**

## I. INTRODUCTION

About twenty years ago the laboratory of Spin-Polarized Electron Spectroscopy (SPES)—the first of its kind in the FSU—was founded at St. Petersburg State Technical University. At that time Professor V. A. Grazhulis at the Institute of Solid State Physics RAS was already interested in this new type of the electronic spectroscopy, and joint activities for the fabrication of modern spin-polarized electron sources were started in 1988 both at the laboratory of Professor Grazhulis and at the SPES laboratory.

In early 1991 a major breakthrough in achieving polarizations of photo-emitted electrons as high as 90 % was made using thin, strained-layer III-V semiconductor structures [1,2]. Today highly polarized electrons from emitters of this type find successful and growing applications in various branches of modern physics [3–5].

This paper presents the state-of-art of spin-polarized photoemission from strained semiconductor heterostructures and gives examples of the applications of polarized electrons in high-energy physics and in the spin-polarized electron spectroscopy studies of surface and thin-film magnetism. The paper is organized as follows. In Section II we review the principles of generation of highly polarized electrons. In Subsection II A the results obtained using strained overlayer cathodes for the polarized electron emission are presented. Subsection II B is devoted to the studies of the polarized electron emission from short-period superlattices. In Subsection II C the peculiarities of the electron kinetics in the band-bending region are discussed, while Subsection II D is devoted to the experimental and theoretical studies of the surface charge limit effect. The applications of the polarized electron beams are discussed in Section III with particular attention–in Subsection III A–to the medium and high energy physics and–in Subsection III B–to the studies of magnetic properties of the materials . Finally, Section IV contains a brief discussion of the prospects of polarized electron sources and some concluding remarks.

## II. GENERATION OF POLARIZED ELECTRONS

It should be noted that in all experiments using polarized electron beams, the principal experimental information comes from the measurement of spin-dependent asymmetries, i.e., the small differences of signal upon reversing the polarization vector, $P$, of the incident electron beam. Therefore, the principal experimental requirement is for an intense electron beam with high polarization and high stability under reversal of the polarization direction. Polarized electron sources based on photoemission from GaAs or its relatives under excitation by circularly polarized light have proven to be the most successful for such experiments.

Photoemitters of highly polarized electrons take advantage of two well-studied physical phenomena in semiconductors: (1) the optical spin orientation of electrons [6] and (2) the sharp lowering the semiconductor surface work function up to a negative electron affinity state under special surface activation procedures [7].

Fig.1a illustrates the principle of optical spin orientation in a cubic GaAs structure. At the Γ-point of the Brillouin zone the wave functions describing conduction band electrons of lowest energy have S-symmetry while those describing valence band electrons at the band edge possess a symmetry of the 4-fold degenerate state with angular momentum $J = 3/2$. Two optical transitions—by photoabsorption of circularly polarized ($\sigma^+$) radiation—to the conduction band, leading to the final state sublevels corresponding to the spin projections $m_s$ = -1/2 and $m_s$ = +1/2, are allowed.

For symmetry reasons the transition probability to the conduction-band state $m_s$ = -1/2 is three times larger than that corresponding to $m_s$ = +1/2, which results in a spin polarization of the conduction band electrons of $P$= -50 %. The electronic spin polarization is defined as $P = \frac{n_+ - n_-}{n_+ + n_-}$ where $n_+$ ($n_-$) is the number of electrons with the spin parallel (antiparallel) to a quantization axis taken along the propagation direction of the incident light. The sign of polarization may be reversed simply by reversing the helicity of the incoming radiation.

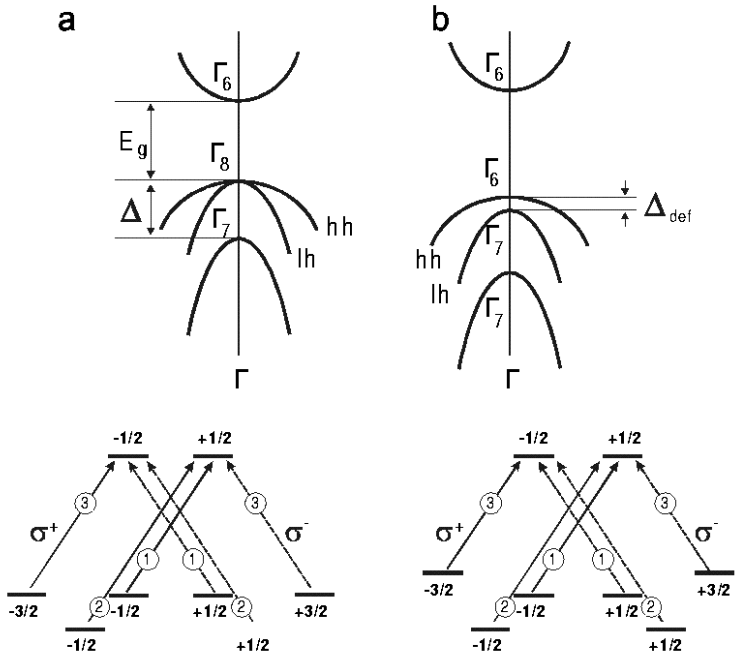


FIG. 1. Optical spin orientation in $A_3B_5$ semiconductor layers: band spectrum near Γ-point of the Brillouin zone in unstressed (a) and in stressed (b) crystal. The arrows indicate interband optical transitions under illumination by the circularly polarized $\sigma^+$ (or $\sigma^-$) light (their relative probabilities are given in the circles), $\Delta$ is spin-orbital splitting of the valence band, $\Delta_{\rm def}$ deformation splitting in a stressed layer.

Emission of electrons is achieved by lowering the electron affinity of the emitting surface. For a strongly p-doped crystal the energy bands are bent downward at the surface thus lowering the vacuum level. Activation of a GaAs crystal by deposition of a submonolayer of Cs + O (or Cs + F) on the atomically clean surface, when combined with the band bending, results in a state of negative electron affinity (NEA) at the surface [7]. When the crystal is biased electrically negative, conduction-band electrons may leave by tunneling through the narrow potential barrier at the NEA surface.

From Fig. 1a it follows that a natural way to increase the polarization of the excited electrons is to eliminate the orbital degeneracy at the top of valence band and selectively excite a single interband transition (see Fig.1b). The degeneracy can be removed by reducing the cubic GaAs lattice symmetry to tetragonal symmetry by applying a uniaxial stress along the [100] crystallographic direction or a biaxial stress in the (100) plane [8]. In recent years

this idea was successfully explored in semiconductor heterostructures with strained thin films for which the lattice mismatch gives rise to substantial stress in the overlayer.

### A. Strained overlayers

In a thin strained GaAs epilayer grown on a thick substrate with smaller in-plane lattice constant, a biaxial compression in the (100) plane increases the mean band gap, moves up the heavy hole band, and pushes down the light hole band (see Fig.1b). The splitting of the $P_{3/2}$ valence-band-maximum multiplet state alters the optical absorption at the band edge, permitting single-band excitation, which leads to a dramatic increase of the polarization compared to that of an unstrained crystal. Due to the small crystal field splitting, the transition probabilities remain nearly the same as in the case of unstrained GaAs. The band gap of the substrate must be chosen to be larger than the gap of the overlayer. Then only electrons from the strained layer will be emitted at the photothreshold. The first results in achieving an electron polarization of $> 50$ % were reported in early 1991 with a strained InGaAs on GaAs buffer substrate [1] and GaAs on GaAsP structures, [2].

To obtain high values of electron-spin polarization, the valence-band splitting in the active layer, $\Delta_{\rm def}$, must be greater than the band-tailing energy in the p-doped sample, which is about 30 meV for a doping level of $N_a = 3 \times 10^{18}$ cm$^{-3}$ at room temperature. A value of elastic strain close to 1 % is generally sufficient to produce the necessary splitting. For such strains the value of the critical thickness of a GaAs strained layer, $H_c$, is about 10-20 nm, $H_c$ being the thickness beyond which strain cannot be perfectly maintained. Since an epilayer thickness of at least 100 nm is needed to support an adequate quantum yield ($Y$), misfit dislocations are introduced during growth when $H_c$ is exceeded, resulting in plastic relaxation.

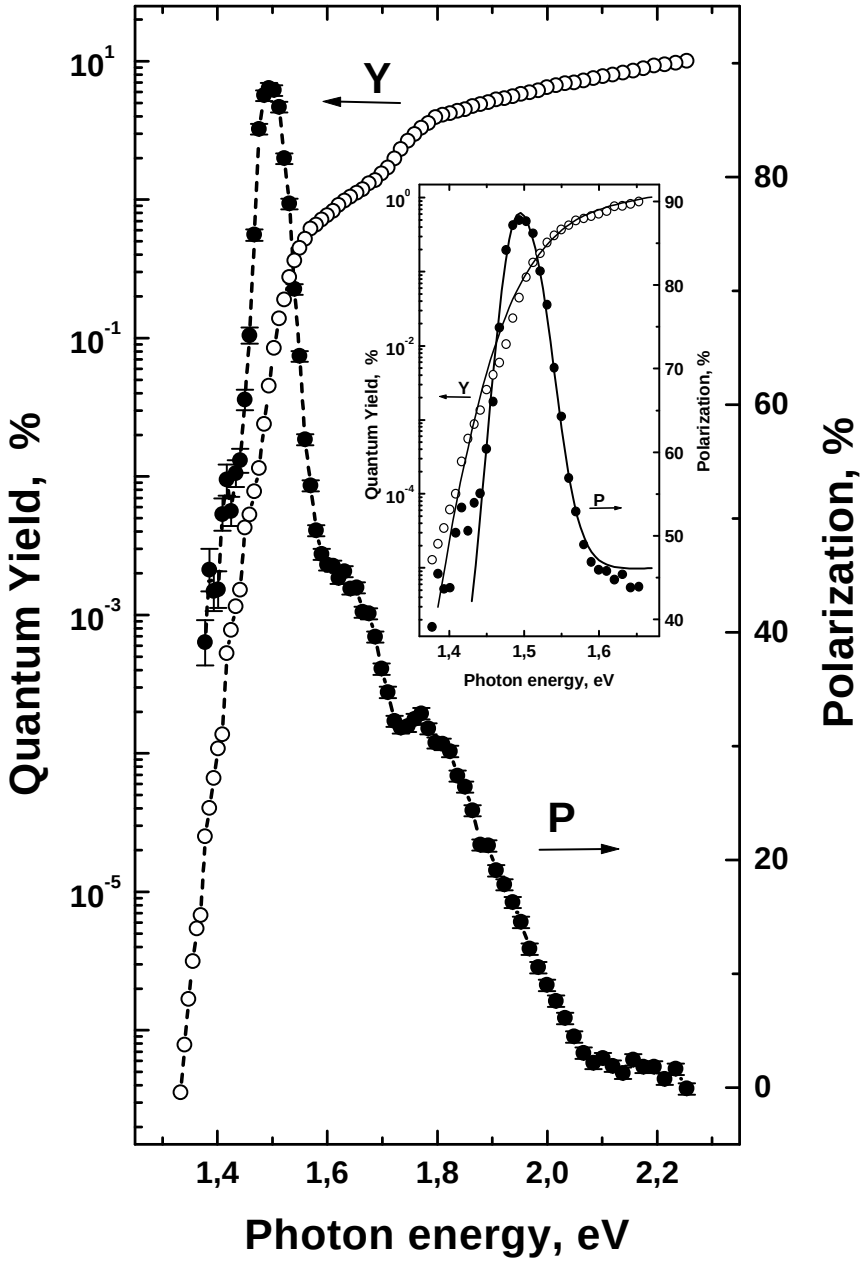


FIG. 2. Electron spin polarization $P$ (full circles) and the cathode quantum yield $Y$ (open circles) as a function of excitation photon energy $h\nu$ for $GaAs_{0.95}P_{0.05}/GaAs_{0.68}P_{0.32}$ strained layer sample at room temperature. (Figure from Ref. [10].) In the inset, the experimental data (circles) are compared with the results of calculations (solid lines) using the diffusion model.

To reduce these relaxation effects, a special type of heterostructure has been proposed [9] comprised of a strained highly p-doped thin GaAs film grown on a GaAsP pseudo-

substrate in such a manner that homogeneity of the stress in the active layer is maintained. A strain-induced energy splitting of $\Delta_{\rm def} \geq 40$ meV in the valence band has been achieved so that today high values of spin polarization of photoelectrons of about 80 % are routinely reached. Metallo-organic chemical vapour deposition (MOCVD) technology appeared to be most suited for the growth of the strained heterostructures with phosphorous-containing compounds.

Fig. 2 from Ref. [10] shows spectral curves of the polarization and the quantum yield that were recently measured at the SPES laboratory at room temperature using a $GaAs_{0.95}P_{0.05}/GaAs_{0.68}P_{0.32}$ strained photocathode. The sample was grown in a horizontal MOCVD reactor on a commercial GaAs (001) wafer and capped with As for protection. The maximum value of $P$ is 88% at $h\nu$ =1.50 eV, the quantum yield at the polarization maximum being equal to $8.5\times10^{-4}$. The typical features of the $P(h\nu)$ and $Y(h\nu)$ curves are clearly seen, i.e., sharp enhancements of $P$ near the photothreshold due to tensile strain along the surface normal, then decreasing of $P$ when $h\nu > E_g + \Delta_{\rm def}$, where $E_g$ is the band gap of the epilayer. In this energy region the electrons are generated both from the heavy hole (hh) and light hole (lh) bands, and the polarization approaches the value of 50%, which is the theoretical limit for the bulk material.

Electron injection from the buffer layer starts to contribute to the emission current at $h\nu \geq$1.8 eV, giving a shoulder in the $Y(h\nu)$ spectrum. Then there is a dip in the $P(h\nu)$ spectrum when the input of the electrons excited from the spin-orbital splitted band with $P = -1$ starts to be noticeable.

The features of the spectra are well understood by now in terms of the band structure shown in Fig. 3a. As a rule, the electron mean free path, $l$, and the thickness of the band bending region (BBR) in the heavily doped p-GaAs layer are much smaller than the absorption length $1/\alpha$ (here $\alpha$ is the absorption coefficient). Therefore the photoemission can be considered a bulk effect that can be described in terms of the three-step photoemission model [11]:

(1) electron excitation under optical pumping,

(2) electron relaxation to the local equilibrium state and diffusion to the BBR, and finally,

(3) electron escape into vacuum throughout the BBR.

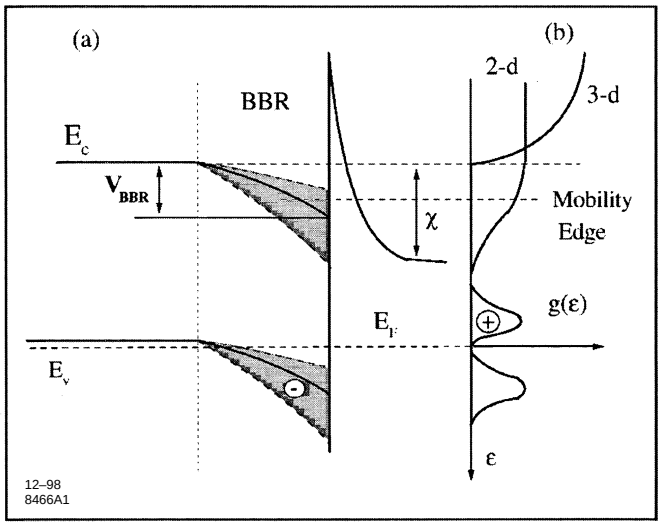


FIG. 3. (a) The electronic energy bands near the activated surface of an NEA GaAs sample, and (b) the density of surface states, $g(\epsilon)$, near the bottom of the conduction band and in the region of the donor states as a function of the localization energy $\epsilon$. $E_c$ and $E_v$ are the energies of the edges of the conduction and valence bands respectively. $E_F$ is the Fermi energy, $\chi$ the electron affinity, and $V_{BBR}$ the average depth of the BBR potential well. The shaded areas in part (a) show the smearing of the band edges by the fluctuation potential.

If the cathode active layer thickness is $d \ll L_D$, where $L_D$ is the diffusion length, and if $S_0$ is the front surface recombination velocity (which is assumed to be much higher than that of the back interface, $S_1$), then the average time of electron extraction from the active layer to the BBR is $\tau_{\rm ext} = d/S_0$. The energy relaxation time by optical phonon emission is a great deal smaller than either the spin relaxation time, $\tau_s$, or $\tau_{\rm ext}$, so the polarization losses during the electron thermalization can be neglected. In addition, experimental studies of the emitted electron energy distribution [12] show that the emitted electron energies are shifted below the bottom of the conduction band. This indicates that most of the photoelectrons are rapidly captured in the BBR well before emission into vacuum.

To obtain high polarization, cathodes with thin active layers must be used such that

$d \ll L_s$, where $L_s = \sqrt{D\tau_s}$ and $D$ is the diffusion coefficient. Therefore in the small absorption region $1/\alpha >> d$, the quantum yield and the electron polarization are given by [13]:

$$Y(h\nu) = (1 - R)\alpha(h\nu)dB_N, \tag{1}$$

and

$$P(h\nu) = P_0(h\nu)\frac{\tau_s}{\tau_s + \tau_{\text{ext}}}B_S, \tag{2}$$

where $B_N$ is the electron escape probability from the BBR and $B_S$ is the probability of escape from the BBR without loss of polarization. It follows from Eqs.(1,2) that near the absorption edge of the active layer (where the contribution of the substrate can be neglected), the $Y(h\nu)$ dependence is similar to that of the absorption coefficient, while the polarization spectrum reproduces the energy dependence of the electron polarization at the moment of excitation, $P_0(h\nu)$. This is not the case when the electrons are excited in the tail states of the conduction band below the mobility edge. In this latter case the electron extraction time is enlarged by the necessity for the electrons to be thermally activated above the mobility edge, and consequently the polarization of the emitted electrons decreases.

The electron polarization at the excitation moment is given by

$$P_0(h\nu) = P_h\frac{\alpha_h}{\alpha_l + \alpha_h} + P_l\frac{\alpha_l}{\alpha_l + \alpha_h}. \tag{3}$$

Here $\alpha_h$ and $P_h$ ($\alpha_l$ and $P_l$) are the partial absorption coefficient and the electron polarization for electron excitation from the heavy-hole (light-hole) band. $P_h(h\nu)$ is a function of the electron energy, which (for $\sigma^-$ excitation) decreases smoothly from +1 to +1/2, while $P_l(h\nu)$ changes from -1 to +1/2. The resulting electron polarization depends on the relative contribution of the light- and heavy-hole bands.

The results of the $P$ and $Y$ calculations in the diffusion model when the smearing of the interband absorption edge due to the band tailing is taken into account [13] are presented in Fig. 2 in the inset by the solid lines. The parameters of the model used in the calculations

are as follows: $L_D = 2\ \mu$m, $D$=40 cm$^2$/s, $S_0 = 4\times10^6$ cm/s, $\tau_s = 5\times10^{-9}$ s, the smearing of the valence band density of states is assumed to be of a Gaussian form and is characterized by the valence band tailing parameter $\gamma_h = 25$ meV.

Band tailing leads to an initial depolarization of the electrons in the conduction band due to the light-hole band contribution to the absorption at the absorption edge of the stressed layer [14], which grows rapidly with the doping of the active layer and gives rise to the polarization anomaly [15] seen in low-temperature luminescence spectra [16].

Eq. (1) predicts a linear growth of the quantum yield with the thickness of the active layer, while Eq.(2) predicts a linear decrease of the maximum polarization. These predictions are in line with the experimental data of Refs. [1,2,9,10,17]. Consequently, Eq. (1) enables one to estimate from the experimental results the surface escape probability for a given value of $Y$ at the polarization maximum, viz., $B_N = Y_{\max}/((1-R)\alpha(h\nu_{\max})d)$. Taking $Y_{\max} = 1\times10^{-3}$ as a typical value for a $d = 0.15$ $\mu$m-thick epilayer and $\alpha(h\nu_{\max}) \approx 10^3$ cm$^{-1}$, we get $B_N \approx 0.5$, which reveals that the electron losses in the BBR of a good cathode are not too high.

As it was noted above, the thickness of the epitaxial layers used for strained-layer cathodes exceeds the critical thickness, so the stored elastic strain in the epitaxial layer is relieved by misfit dislocations. For the zincblende structure, misfit dislocations develop asymmetrically along the two orthogonal directions [110] and [1$\bar{1}$0], resulting in an anisotropic (shear) strain within the plane of the epitaxial layer. The shear strain induces an optical anisotropy of the strained-layer structure which manifest itself in spin polarization resonances when the photocathode is a part of an all-integrated Fabry-Pérot optical cavity [18].

The shear strain will mix the heavy-hole and light-hole split-off valence states and affect the optical transition probabilities. Since the mixing occurs only between opposite $m_j$ states, if the excitation light is 100 % circularly polarized, only one state can be excited, and the electron-spin polarization will be unaffected. However, if the excitation light is linearly polarized, more than one state can be excited and the excitation probabilities will be dependent on the direction of linear polarization resulting in a quantum efficiency anisotropy.

The shear strain and anisotropy of the photocathode quantum efficiency as a function of the degree of strain relaxation was investigated in Ref. [19].

The existence of a $Y$ anisotropy in strained-layer photocathodes used for PES may lead to helicity dependent intensity variations if there exists a small, unintentional, linear component in the circularly polarized light. Fortunately, it can be compensated by optical means.

### B. Short-period strained superlattices

Various studies of strained-layer cathodes (e.g. [1,2,9,16–19]) indicate that further improvements are limited by the controversial character of the demands on the cathode heterostructure parameters. For most applications a high yield is required, which implies a certain minimal epilayer thickness. Concurrently a high polarization is required [20], which implies a high stress in the epilayer. Highly stressed layers have small critical-layer thicknesses beyond which the strain gradually relaxes due to structural defects. These defects will lead to the growth of the spin relaxation rate and thus polarization losses.

An alternative source of highly polarized electrons that has a potential for further development is found in superlattice (SL) structures, especially in the so-called strained short-period SL with specially designed layer thicknesses and compositions [21–24]. They consist of several (10-20) thin strained films (for example, InGaAs) separated by layers of unstrained larger-bandgap material (GaAs or AlInGaAs) specially designed to build barriers for the hole transport but keeping electron mobility high. These structures can be grown by molecular beam epitaxy (MBE). From the point of view of growth of a perfect crystal, every separate strained film of the SL can be grown smaller in thickness than the critical thickness, but the total thickness of all the strained films can have a value considerably larger than $H_c$ and will be sufficient to obtain high $Y$ values. The other benefit of an MBE-grown SL is the supplemental splitting of the heavy-hole and light-hole minibands in the valence band caused by hole localization in SL quantum wells (QW) that can (in the case of deep and narrow QW for holes) exceed the splitting caused by stress. In addition, MBE technology

gives the possibility of precise modulation doping of the active layer (low average doping concentration and high concentration in the BBR), which results in smaller polarization losses during electron escape from the active layer and the BBR into vacuum.

During the past few years, several strained $Al_xGa_{1-x}As$ / $In_yGa_{1-y}$ As (x=0.15; y=0.1 to 0.15 to vary the value of the strain) SL structures were studied [21–24]. The measured room temperature spectra, $P(h\nu)$ and $Y(h\nu)$, and the yield logarithmic derivative, $d(\ln Y)/d(h\nu)$, from Ref. [23] are shown in Fig. 4. The sharp peaks both in the $Y$ derivative and the $P$ spectra are clearly seen. The peaks are attributed to the onset of optical excitation from the corresponding SL miniband. The quantum yield is, in general, proportional to the light absorption coefficient of the material, which is in turn proportional to the joint conduction-valence-band density of states. The density of states of the superlattice has van-Hove singularities at every miniband edge. The singularities are manifested as peaks of the $Y$ derivative.

The polarization peaks are of a different nature. Their appearance is to be understood as the evidence of the dominant contribution of the excitation of the corresponding miniband in the peak area, since at the edges of interband optical transitions between the minibands, the electrons are highly polarized. The peaks are shifted from the very edge to the high-energy side where the absorption is high. The theory of electron optical orientation in semiconductor quantum well structures and the contribution of the various subband transitions was developed for the case of infinitely deep quantum wells by Merkulov et al. [25]. Their arguments for high polarization at the edges of the allowed optical transitions are valid also for superlattices with deep quantum wells for holes and should be combined with the arguments on the relative contribution of the different excitation channels to the resulting electron yield. The effective periodic potential formed by the band-edge variation in the SL results in the miniband energy-spectrum formation. The positions of the peaks and dips in the polarization spectrum are found to be in reasonable agreement with the inter-miniband transition energies deduced from the miniband spectrum, calculated using

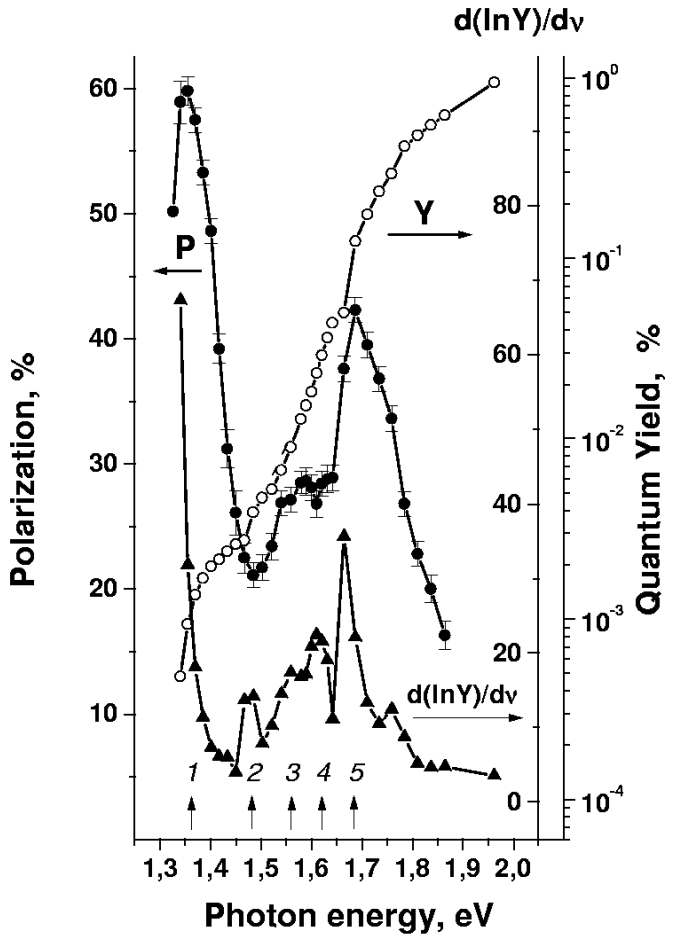


| № | Transition | Energy [eV] | Spin orientation |
|---|---|---|---|
| 1 | $hh_1 \rightarrow e_1$ | 1.36 | ↑ |
| 2 | $lh_1 \rightarrow e_1$ | 1.48 | ↓ |
| 3 | $hh_2 \rightarrow e_1$ | 1.56 | ↑ |
| 4 | $hh_1 \rightarrow e_2$ | 1.62 | ↓ |
| 5 | $hh_2 \rightarrow e_2$ | 1.68 | ↑ |

FIG. 4. Dependence of the electron spin polarization $P$ and quantum yield $Y$ on the optical excitation energy at room temperature for an $In_xGa_{1-x}As/Al_yGa_{1-y}As$ SL sample. The dependence of the logarithmic derivative of yield, $d(\ln Y)/d(h\nu)$, is also shown. (Figure from Ref. [23].) The onsets of the inter-miniband transitions listed in the Table are shown by the arrows.

the envelope-function approximation, in the framework of the Kane model, including the conduction band $\Gamma_6$ and the states of light and heavy holes of the valence band $\Gamma_8$ and the

spin-orbit (SO) band $\Gamma_7$ [26].

To estimate the prospects of the SL based structures as photoemitters for a PES, one can consider a superlattice to be a new semiconductor material with parameters that can be varied by the choice of the composition and thickness of the layers, so that the results of the diffusion model for the photoemission can be applied [27]. Therefore, in accordance with Eqs. (1,2), the basic parameters of the photocathode structure are $\Delta_{\rm def}$, $\tau_s, S_0$, and $\alpha$, whereas $B_S$ and $B_N$ are more sensitive to the properties of the BBR and the surface activation layer.

*Valence band splitting.* High initial electron polarization, $P_0$, upon excitation by circularly polarized light requires a large splitting, $\Delta_{\rm def}$, of the heavy and light valence band states. The hole miniband spectrum calculations as a function of the layer thickness and composition in the framework of multiband Kane model [26] show that the light- and heavy-hole miniband splitting is enlarged in a SL with a high value of the valence-band offset, $\Lambda_v$, at the heterointerfaces. In the InGaAs-AlGaAs and to much larger extent in the GaAs-InGaP SL, the ratio $\Lambda_v/\Lambda_c$ (where $\Lambda_c$ is the conduction-band offset) is considerably higher then that in a traditional GaAs/AlGaAs SL. As a result a value of splitting as large as $\Delta_{\rm def} \approx$ 80-100 meV can be achieved for the SL layer thicknesses of $a \approx b \approx 3$ nm. These results are consistent with experimental findings in the photoemission and photoreflection spectra of these SLs [23,24,28].

*Spin relaxation rate.* The mechanisms of the spin relaxation in $A_3B_5$ semiconductors were amply documented in Refs. [31,32]. At low temperatures and in the highly p-doped crystals, the spin-relaxation mechanism due to the electron-hole exchange interaction proposed by Bir, Aronov and Pikus (and commonly denoted as the BAP mechanism) dominates [31]. In a SL the effective interaction Hamiltonian can be obtained by averaging over the SL period, which results in $H = H^{(a)}P_a + H^{(b)}P_b$, where $P_a$ and $P_b$ are the probabilities of an electron to be in $a$-thick and $b$-thick layers respectively. Therefore in a short-period SL with a small spin relaxation rate in the barriers, the resulting spin relaxation rate can be considerably reduced.

At room temperature in crystals with low or moderate doping level the spin precession mechanism proposed by D'yakonov and Perel' (the DP mechanism) prevails [32]. A considerable modification of the DP spin relaxation in a SL should be taken into account [29]. The effective Hamiltonian for the i-th layer can be written as

$$H_{\mathrm{prec},i} = \frac{1}{2}\alpha_i(\hat{\sigma}_y k_y - \hat{\sigma}_x k_x)\frac{\hbar^3 < k_z^2 >}{(2m_i E_{g,i})^{1/2} m_i}, \quad i = a, b \tag{4}$$

where $\alpha_i$ is the interaction constant, $\hat{\sigma}_{x,y}$ are the Pauli matrixes, $k_n, n = x, y, z$ are the components of the electronic wave vector, $m_i$ is the electron effective mass, and brackets mean averaging over electron transverse motion in the layer. The spin relaxation rate in the SL is given by

$$\frac{1}{\tau_s} = \frac{\beta^2 k_b T}{2\hbar^2 \nu_p E_g}, \tag{5}$$

where

$$\beta = \left(\frac{\alpha_a \hbar^2 q^2}{m_a}\right) P_a - \left(\frac{\alpha_b \hbar^2 \kappa^2}{m_b}\right) P_b, \tag{6}$$

$q^2 = 2m_a(E - E_{c,a})$, and $\kappa^2 = 2m_b(E_{c,b} - E)$, $E$ is the electronic state energy, $E_{c,a}$ and $E_{c,b}$ the conduction band edges in the layers, and $\nu_p$ is the momentum relaxation rate, $P_a$ is the probability to find the electron in the layer $a$, $P_b = 1 - P_a$. It follows from Eqs. (5,6) that in a SL with high barriers for the electrons (and a large value of $< k_z^2 >$ in one of the layers), the spin relaxation due to the DP mechanism can be much faster than that due to the BAP mechanism. It is a linear function of temperature and is strongly dependent on the parameters of the SL layers, viz., compensation of the precession in wells and barriers is possible [29]. In a SL with small barriers for the electrons (small values of $< k_z^2 >$ in both layers), the DP mechanism is suppressed near the first conduction miniband minimum.

Estimates for a GaAs-$Al_{0.3}Ga_{0.7}As$ SL with a=b=3 nm, $\alpha_i \approx 0.07$ and $\nu_p \approx 10^{13}$ $s^{-1}$ give $\tau_s \approx 7 \times 10^{-11}$ s, which is comparable with the relaxation rate due to the BAP mechanism. However the DP relaxation rate is much smaller in an InGaAs-GaAs SL and other SL structures with a conduction-band offset smaller than 100 meV.

*The surface recombination velocity* is determined by $S_0 =< |v_n| > P_{\rm BBR}$, where $< |v_n| >$ is the average electron velocity in the direction parallel to the surface normal, and $P_{\rm BBR}$ is the probability of electron capture in the band bending region. An estimate based on the envelope-function approximation showed that for superlattices with thin ($\leq 4$ nm) barriers and a conduction band offset less than 100 meV, the escape to the BBR is not slowed down noticeably by the SL barriers, but the slowing becomes important for larger values of the conduction-band offset, $\Lambda_c$.

*Edge absorption* in SL structures can be estimated taking into account both the modification of the electron and hole effective masses and the changing of the optical interband matrix element. As a result of a larger optical (interband) density-of-states effective mass in SL structures, the one-band absorption is expected to be 2-3 times larger than in the stressed single-layer GaAs structures. The optical interband matrix element is reduced in highly p-doped samples by the screening of the the excitonic enhancement effect. Therefore, additional increases in the edge absorption are expected in moderately doped active SL layers due to stronger excitonic effects in SLs.

*Zero conduction-band offset.* The above discussion of the SL parameters that are crucial for the polarized electron emission–$\Delta_{\rm def}$, $\tau_s$, $S_0$, and $\alpha$– indicates that SL structures with large valence band offsets and small conduction band offsets are expected to have much better properties as polarized electron emitters [27], while the thickness of the SL active layer is restricted mainly by the spin losses during extraction to the BBR.

The main advantage of the $Al_xIn_yGa_{1-x-y}As$/GaAs SL proposed in Ref. [30] comes from the band line-up between the semiconductor layers of the SL. The Al content determines the formation of a barrier in the conduction band, while adding In leads to conduction-band lowering, so the conduction band offset can be completely compensated by the appropriate choice of x and y, while barriers for the holes remain uncompensated. Therefore the use of superlattices with an optimized quaternary alloy composition can provide a high vertical electron mobility and simultaneously a small spin-relaxation rate while also maintaining a large enough valence-band splitting.

A calculation of the positions of the $E_c$ and $E_v$ band edges in the layers (following the approach of Ref. [33]) in the strained SL samples with $a = b = 4$ nm on a GaAs substrate showed that the calculated conduction band offset does not exceed 20 meV in samples with close values of x and y. For thermalized electrons at room temperature, the influence of the resulting periodical potential should be negligible, i.e., the low 4-nm-thick barriers for the electrons in the SL will be transparent. Thus changes of electron mobility and spin relaxation rate (compared to pure GaAs) will be small.

The choice of the layer thickness is dictated by the need to split the hole minibands. The splitting grows when barriers are broad enough and wells are narrow and deep. Still the thickness of the strained $Al_xIn_yGa_{1-x-y}As$ layer (which acts as a barrier for the holes) should be less than the critical thickness $h_c(y)$. The overall critical thickness $H_c$ for the SL with alternating layers of equal thickness can be estimated if one considers the whole SL layer as a unity with an average lattice constant. Then, the misfit between the substrate and the active layer is two times smaller than between the two contacting layers, so that $H_c = h_c(y/2)$.

The thickness of a single $Al_xIn_yGa_{1-x-y}As$ layer in Ref. [34] was taken to be 4 nm (to be less than the calculated $h_c(y)$). The thickness of the whole active layer $d = 0.12 - 0.13$ $\mu$m according to X-ray data, exceeded $H_c$ much less than in the case of a cathode structure with one strained GaAs layer, since only minor strain relaxation effects in X-ray spectra were observed.

In Fig. 5, the measured polarized emission and quantum yield data for a SL sample with minimized conduction-band offset are shown as a function of the optical excitation energy [34]. The surface dopant density of $4 \times 10^{18}$ cm$^{-3}$ was decreased an order of magnitude in the bulk to reduce depolarization effects. The maximum polarization obtained was 86 % and the quantum yield at the polarization maximum, $Y_{\max}$, was $7.5 \times 10^{-3}$. $Y_{\max}$ is found to be sensitive to the activation procedure and the vacuum conditions. Measurements with better vacuum gave $Y_{\max} = 9.4 \times 10^{-2}$ (for a somewhat lower polarization of 82.7 %), which is at least an order of magnitude better than obtained with other cathode structures. Thus,

modulation doping of the SL with minimized conduction band offset provides both high polarization and high quantum yield at the polarization maximum.

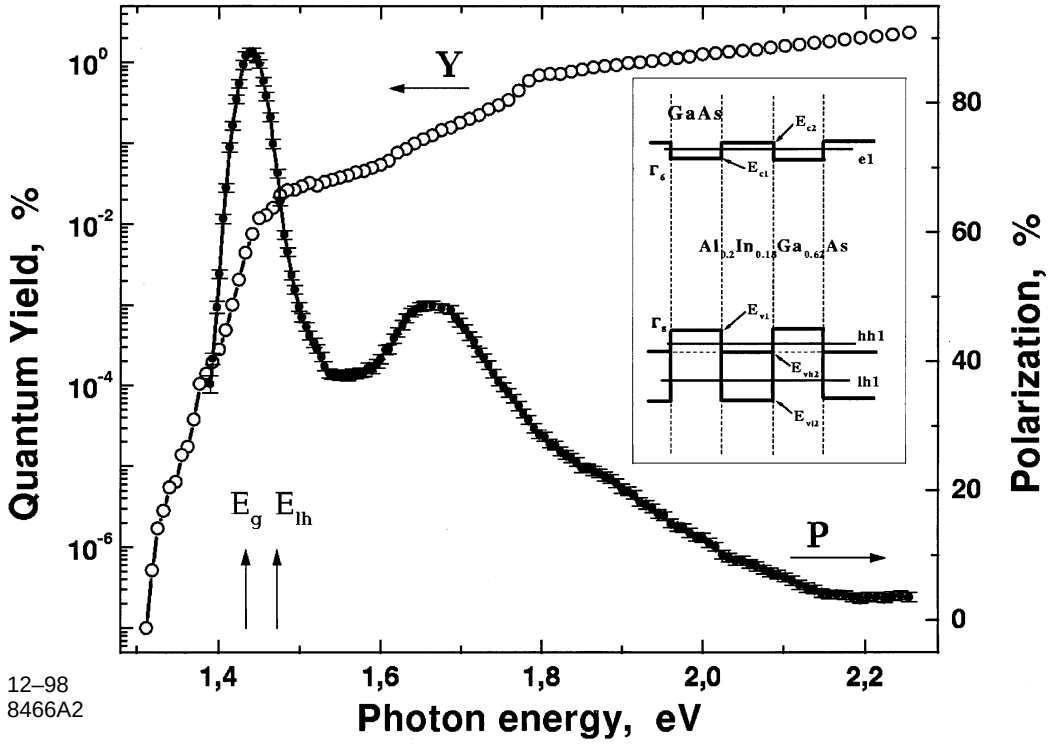


FIG. 5. Electron spin polarization and quantum yield as a function of excitation energy for an $Al_xIn_yGa_{1-x-y}As$/GaAs SL sample. The band gap energy, $E_g = E_{e_1} - E_{e_{hh1}}$, and the light hole excitation energy, $E_{lh} = E_{e_1} - E_{e_{lh1}}$, are indicated by arrows. The energy band diagram of the SL is shown in the inset. The minibands (thin lines) are identified by the notation e1 and hh1, lh1 for electrons and holes respectively. (Figure from Ref. [30].)

The position of the polarization maximum is close to the SL band gap. The value of the band gap in the SL is larger than that in the GaAs layers due to the quantization energy of the heavy holes and some shift of the conduction band minimum. A calculation of the miniband energies using the model described in Ref. [26] gives the hole-miniband energies $E_{hh1} = 13$ meV and $E_{lh1} = 54$ meV. The difference of these values gives a valence band splitting that is consistent (within the errors of determination of the band edges) with the observed width of the polarization maximum. The edge of the electronic band in a SL

with a small conduction-band offset is close to the average conduction-band energy in the contacting layers.

Note that the calculation of the band gaps for SLs with different layer compositions using the SL layer parameters evaluated as in Ref. [33] gives for all samples values that differ from the experimentally observed energies of the polarization maximum (exceeds it) by $\approx 20$ meV. The regular difference in the calculated and observed band gap values in the strained quaternary alloys can be attributed to the uncertainties in the conduction-band offset calculations and also to some tensile deformation of the GaAs layer resulting in less strain in the contacting $Al_xIn_yGa_{1-x-y}As$ layer. This misfit can be rather easily corrected by choosing a SL with larger x when some tuning of the SL band gap to the excitation source is needed.

Indeed, adding Al does not influence the deformation so that the band gap variation with x is predictable. It may be remarked that one can expect a smaller spin relaxation rate for a SL with an optimally chosen doping profile that is compatible with needed extracted emission current. Thus optimization of structure parameters and the doping profile can lead to further improvement of the proposed new SL photoemitter structure.

### C. Electron kinetics in the band-bending region

The three-step emission model discussed earlier includes as phenomenological parameters the electronic escape probability from the BBR in vacuum, $B_N$, and the probability of the electron escape from BBR without loss of polarization, $B_S$. The values of these parameters set limitations on the maximum polarization and yield values of the cathode structures. Therefore the BBR appears to be a bottleneck for progress. It is even more so for the case of the high intensity excitation when a photovoltage is build up in the BBR that reduces the NEA and $Y$ values.

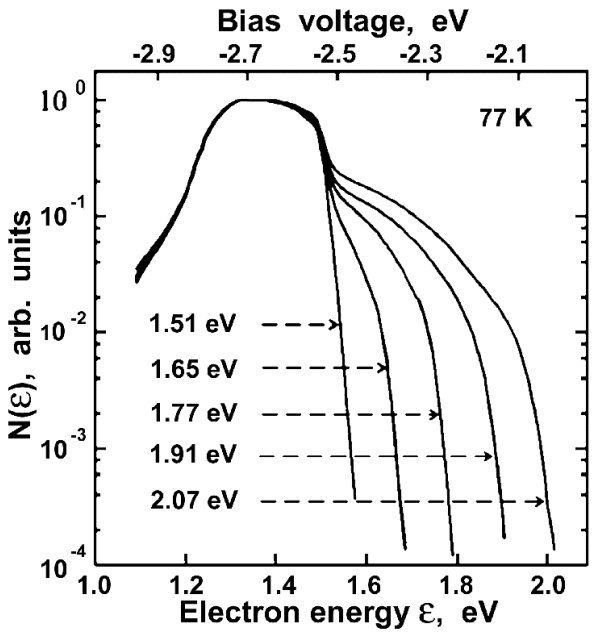


FIG. 6. Electron energy distribution curves of GaAs unstrained cathode, normalized to the maximum value for several excitation energies (measured by the parallel plate retarding field analyzer). (Figure from Ref. [12].)

The character of the electron kinetics in the BBR is still a rather controversial matter. The main information bearing on this situation comes from studies of the emitted electron energy distribution curves (EDC) [35] and the polarized electron energy distribution curves (PEDC) [35]. Detailed investigations of the EDC [12,35–37] both at room and low temperature reveal that the electron energy distribution is spread over a broad energy band with a width of ≈300 meV (close to the value of NEA) shifted below the position of conduction-band minimum in the bulk. Typical EDC measured for an unstrained GaAs 0.2 $\mu$m-thick sample with a doping level of $N_a = 6 \times 10^{18}$ cm$^{-3}$ at several energies of exciting photons are shown in Fig. 6. The broad electron energy distribution implies a long stay of the electrons in the BBR during the emission process. Studies of the charge limitation phenomena [38] give additional evidence of the slowness of the BBR kinetics compared to the rate of energy relaxation by emission of optical phonons. Still, the polarization of the emitted electrons remains high. In Fig. 7 PEDC for an unstrained GaAs sample measured at different pho-

ton energies [35] are depicted. The experimental PEDC show (in addition to the features in high-energy region above the conduction-band bottom ascribable to the details of the crystal band structure) rapid switching off of the depolarization for low-energy electrons. This observation contradicts the expected strong electron depolarization due to the DP mechanism in the effective magnetic field that is present in the BBR [40].

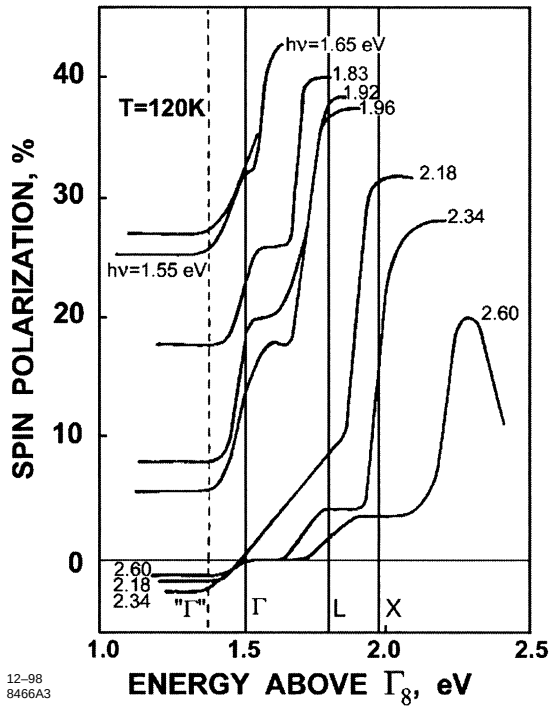


FIG. 7. Polarized electron distribution curves for GaAs unstrained cathode for several excitation energies $h\nu$. The energies of the $\Gamma$, $L$ and $X$ valleys in the conduction band are shown by vertical lines. (Figure from Ref. [39].)

An efficient mechanism of electron energy relaxation in GaAs is the emission of polar optical (PO) phonons (or polar surface phonons). The electron-hole scattering process in which a heavy hole is scattered to the light-hole subband is less effective in the BBR than in the bulk due to the spatial separation between electrons in the BBR and holes in the bulk. The emission time of one optical phonon in a GaAs surface BBR is less than $\tau_{\rm PO} = 1.5\times10^{-13}$ s [41]. The estimated time of the electron emission from the BBR into vacuum is $\tau_{\rm emi} = \hbar/(T\delta E)$, where $\delta E$ is the energy distance between the electronic levels in an average

BBR potential well, and $T$ is a surface barrier transparency. For a low transparency barrier, $T \approx 2$ %, and $\tau_{\rm emi} \approx 0.5 - 1.5 \times 10^{-11}$ s, so that $\tau_{\rm po} \ll \tau_{\rm emi}$. Thus the thermalization of electrons in the BBR could be very rapid.

Note that both times $\tau_{\rm po}$ and $\tau_{\rm emi}$ are considerably smaller than the electronic lifetime in the BBR. Therefore, one could expect a strong distinction between "bad" cathodes having insufficient NEA so that the minimal electron energy in the BBR is below vacuum level and "good" ones with high NEA (vacuum level is below the least electron energy in the BBR). The former structures could have low quantum yield and high electron polarization, while the letter should have quantum yield close to unity but low polarization. This conjecture contradicts the smooth spread of Y values observed experimentally for different cathodes after activation and during temporal degradation, and also the rather rather weak correlation observed between P and Y values.

We recall here that the BBR-well formation results from the Fermi level pinning on the donor-like Cs-originated surface centers via the electron redistribution between the acceptors (randomly situated near the surface) and the donors. Monte-Carlo modelling of the spatial distribution of the electron potential and the NEA state formation [42,43] turns up large fluctuations of the electronic potential at the surface, implying that all the electronic states in the BBR below a certain energy level are localized in the surface plane by the potential fluctuations. The position of this level defines an electron mobility edge (ME), which in the case of low doping coincides with the position of the percolation level in the fluctuating surface potential [44].

This localization has vital consequences for the electronic dynamics in the BBR, slowing down all the kinetic processes in the BBR below the ME. The edges of the electronic bands smeared by the fluctuations and the density of states in the BBR are shown in Fig. 3 a and b respectively. Note the shift of the ME upwards from the average value of the surface potential due to the quantization of the electronic transversal motion in the BBR well.

The fluctuations in the spatial distribution of the acceptor and donor centers give rise to a fluctuation-electronic potential responsible for the existence of the mobility edge for the

electronic states in the BBR and the tail in the density of the localized states [44], which slows down the electron kinetics. The energy scale, $\delta$, of the fluctuations at the surface can be estimated as $\delta = 2e^2 N_a^{1/3}/\kappa$, where $N_a$ is the acceptor concentration and $\kappa$ is the dielectric constant. The electronic surface-potential fluctuations, $\gamma$, range from $\delta$ to $\gamma = (\delta^3 V_s)^{1/4}$, $V_s$ being the average BBR well depth at the surface, which depends on the activation layer structure [4]. For $V_s = 0.4$ eV and $N_a \geq 3 \times 10^{18}$ cm$^{-3}$, we have $\gamma \geq 100$ meV.

Let us discuss here the position of the EDC maximum [45,46]. The density of the localized electronic states in the BBR, $\rho(\epsilon)$, will be a decreasing function of the localization energy, $\epsilon$, in the band gap. It is convenient to approximate $\rho(\epsilon)$ by an exponent:

$$\rho(\epsilon) = \rho_0 \exp(-\epsilon/\gamma), \tag{7}$$

where $\rho_0$ is the density of states at the ME energy.

Below the ME, phonon emission is possible only in hopping processes between potential wells that have electronic levels separated by an energy smaller than the optical phonon energy and that are, therefore, well separated in space. As a result the electronic relaxation rate slows down together with the density of the final states, so that the EDC will be formed as a result of competition between the processes of electron emission in vacuum and electron hopping in tail states. We will assume the probability of an electron to emit a phonon, $w$, to have an exponential dependence on the hopping distance $r$:

$$w(r) = w_0 \exp(-2r/a), \tag{8}$$

where $w_0 = 1/\tau_{\rm po}$ and $a$ is a localization radius of the hopping electron, which is close to the Bohr radius of the localized state and is a slowly varying function of energy. The time of the electron emission from the BBR in vacuum, $\tau_{\rm emi}$, will be assumed to be constant.

Using Eqs. (7) and (8) one can estimate the position of the maximum of the EDC, $\epsilon_{\rm max}$. For the case when $\gamma \gg \hbar\omega_{\rm po}$, the average hopping distance $r$ between the localized states within the small energy range of $\hbar\omega_{\rm po}$ at the energy $\epsilon$ can be found from the equation:

$$\pi r^2 \rho(\epsilon) \hbar\omega_{\rm po} = 1. \tag{9}$$

The maximum of the EDC is achieved when the probabilities of electron hopping and electron emission into vacuum are equal (i.e., when $w(r)\tau_{\rm emi}$=1), which leads to

$$\epsilon_{\rm max} = \gamma \ln[\frac{\pi}{6}\hbar\omega_{\rm po}\rho_0 a^2 \ln^2(w_0\tau_{\rm emi})]. \qquad (10)$$

Electrons with a localization energy smaller than $\epsilon_{\rm max}$ descend down in energy faster than they can tunnel into vacuum, while below $\epsilon_{\rm max}$ the electrons appear to be in isolated localized states and are preferably emitted. The density of these states and therefore the number of emitted electrons is smaller than at $\epsilon_{\rm max}$.

The $B_N$ factor in Eq. (1) depends on the relative position of $\epsilon_{\rm max}$ and the vacuum level and varies from a value close to unity when $\epsilon_{\rm max} \ll \chi$ (where $\chi$ is the NEA value) to much lower values for cathodes with a surface barrier of low transparency.

Eq. (10) is valid for a low intensity of optical excitation, when the filling factor of the states in the band tail remains small. It follows from Eq. (10) that when $\ln^2(w_0\tau_{\rm emi}) \gg 1$, the shift of $\epsilon_{\rm max}$ can be $\geq \gamma$.

The main mechanism of spin relaxation in the BBR is the DP mechanism. For the localized states below the ME, the diffusion of the spin precession axis together with the directions of the electron motions is suppressed and the DP mechanism ceases to be effective. Estimates show [45] that the spin relaxation is switched off below the ME in an interval of the order of 20 meV, which is in line with the experimental data for the polarized electron energy distribution [35].

Thus the surmise of the electron localization in the BBR well plane (based on the modelling results) can account for a wide electron energy distribution that is shifted down from the conduction band edge, switching off the spin relaxation rate in the BBR, and can be used for more detailed theoretical predictions [45] for the electron distribution and its evolution under intense optical pumping, temperature dependence of the electronic distribution, etc.

Time-resolved measurements of the emitted electron energy distribution and polarization can be very informative to clarify the mechanisms of the electron kinetics and the polarization losses. The assumption of phonon emission as the only mechanism of energy losses in the

BBR (in relatively small amounts) implies a steady electronic drift down in energy.

For thin cathode structures, when the electronic extraction time to the BBR is small, time-resolved measurements will follow this energy degradation (the inverse of the well known hot-electron luminescence technique). Experimental time-resolved studies with picosecond pulses are now in progress [47], though the results obtained by now are not well understood. A typical time-resolved emission profile and phase-resolved polarization for the same type strained-layer cathode structure as in Fig. 2 are depicted in Fig. 8.

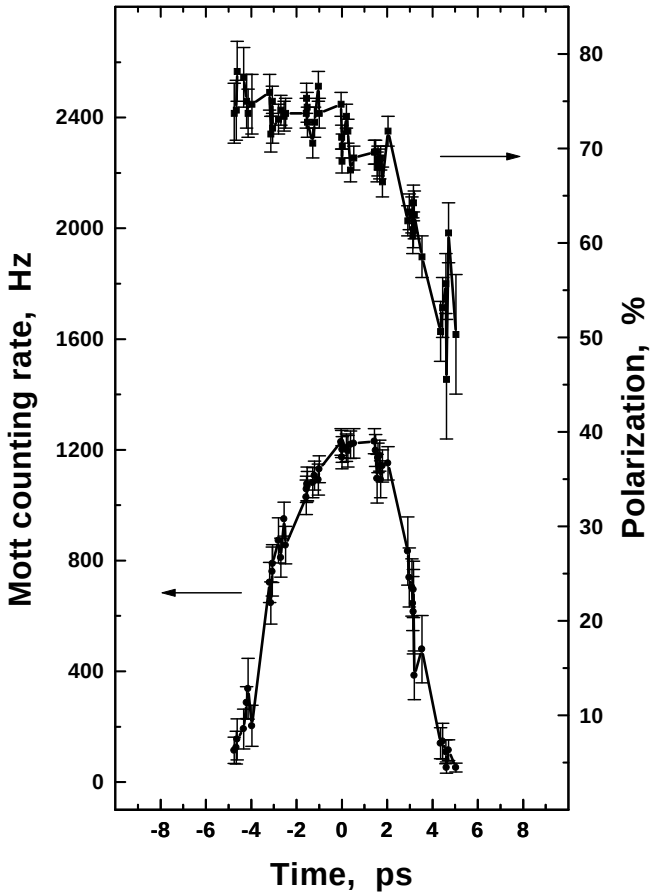


FIG. 8. Emission pulse profile and the phase-resolved polarization from a $GaAs_{0.95}P_{0.05}/GaAs_{0.68}P_{0.32}$ strained layer sample with 0.15 $\mu$m-thick epilayer. (Figure from Ref. [47].)

The measurements were done at Mainz [47] using a laser pulse duration of 1.3 ps at the maximum of the polarization curve. For a 150-nm strained-layer cathode with $Y =$

$4 \times 10^{-4}$, the polarization was found to vary over the 6-ps emission time of the bunch from an initial value of 78 % to a final 50%, giving some justification for the conclusion about the initial polarization losses and their evolution with the electron dynamics. However, the observed decrease of polarization was far from exponential (i.e., the decrease was slower at the beginning of the emission pulse and more rapid at the end), making it difficult to extract the time constants. The unexpected shape of the polarization decay function could be an experimental artefact associated with reaching the time resolution limit of the apparatus. To improve the precision of the determination of the depolarization time constants, additional measurements with improved time resolution are needed.

### D. Surface charge limit effect

Achieving high values of emission current and charge (in the case of pulsed excitation) requires intensive optical pumping. Various experimental groups have observed current saturation and emission charge limitation effects in quasistationary and pulsed excitation regimes respectively [38,48–51].

In Fig. 9 photoemitted charge from a 0.3 $\mu$m-thick strained GaAs cathode doped with Zn to a concentration of $5\times10^{18}$ cm$^{-3}$ for a 2 ns pulse excitation is presented [38]. The charge versus pulse energy dependence becomes increasingly nonlinear as the pulse energy increases, so that in the charge limit regime even a decrease of the emitted charge with the increase of the pulse energy can be obtained. The observed limitations of emission at high excitation are attributed to the photovoltage effect [52].

Qualitatively, the excited electron flow to the BBR reduces the surface charge which decreases the surface band bending, resulting in a decrease of NEA that can be described in terms of a photovoltage (PV). The PV formation is defined as a change in the average depth of the BBR well, $\delta V = V_s^{(0)} - V_s$ [52], where $V_s^{(0)}$ ($V_s$) is the average BBR well depth at the surface without (under) illumination. The PV shifts down the conduction-band minimum relative to the vacuum level and thus, reduces NEA, $\chi = \chi^0 - \delta V$, preventing electrons

from escaping into vacuum. The effect is sensitive to the starting value of NEA, $\chi^0$, without illumination and therefore to the quantum efficiency of the cathode in the linear regime.

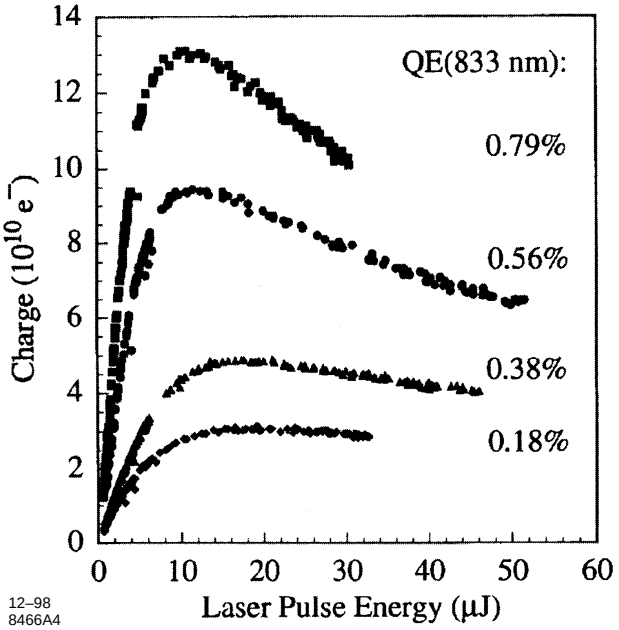


FIG. 9. Emitted charge in a pulse as a function of the optical excitation pulse energy for a strained GaAs-layer cathode for several values of the cathode quantum efficiency (yield). (Figure from Ref. [38].)

The onset of the PV is regulated by the difference in the flow of electrons and holes to surface centers. While the excess electron concentration is formed by electrons that are captured in the BBR and have not had enough time (or energy) to be emitted into vacuum, the main contribution to the hole restoring current to the surface is found to be [49,51] the tunneling current through the BBR barrier for holes (see Fig. 3a), but not the thermionic current, since experimentally the surface charge limit (SCL) effect depends strongly on the doping level but is not very sensitive to temperature.

The kinetics of the SCL have been studied theoretically in Refs. [52,54]. Following the switch-on of the excitation light, the transient time to the stationary values of PV and $Y$ can be estimated as $\tau_{ad} \approx N_s/(I_i \alpha d)$, where $N_s$ is the ionized donor surface concentration and $I_i$ is the maximum illumination intensity. The transient time determines both the electronic

charging of the surface and the diminishing of the barriers for holes. For a sufficiently intense excitation and as a result of the adjustment of the emission current in response to the PV, the dependence of Y on time transforms during the increase of the light intensity from a monotonous increase to a specific peaked form with a width of $\tau_{ad}$. For increasing values of the maximum excitation, the difference between maximum and minimum Y-values increases while the stationary value of $Y$ decreases toward zero. In line with the arguments above, the transient time is observed experimentally to decrease inversely with $I_i$ [50].

On the other hand, there are two stages of restoration of the photocathode characteristics after the switch-off of the illumination. The first stage develops on the diffusion time scale. It is connected with the electron diffusion from the active region in the absence of photogeneration. After this period the width of the BBR and the barrier height for holes increase, and the relaxation proceeds in a linear regime while the photovoltage decreases from a value of approximately 0.1 eV till its value becomes less than $kT$ (second stage).

Integration of the kinetic equation for recombination gives the time dependence of the photovoltage at this stage. Evaluation of the relaxation time gives $\tau_t = (\alpha_p N_* T_h)^{-1}$, where $\alpha_p$ is the hole capture coefficient to the neutral centers with $N_*$ concentration at the surface and $T_h$ is the BBR barrier transparency for holes.

The time $\tau_t$ decreases in inverse proportion to the hole capture coefficient and, via the $T_h$ factor, grows exponentially with decreasing square root of the acceptor concentration. The influence of the remaining photovoltage at the barrier on the photocathode characteristics reveals itself in the investigations of the two-pulse (and multi-pulse) excitation regime. The emission charge in the second pulse is determined both by the change of barrier parameters due to the first excitation pulse and by the relation between the time delay and the restoring time of the barrier characteristics. Both these factors depend on the coefficient of hole capture to neutral centers.

Comparing theoretical dependency of the emitted charge on the laser pulse energy with experimental results (given in Refs. [49,51]) allows one to establish the main parameters of the photocathode structure [54], namely, the electron affinity, $\chi^{(0)}$, the surface potential well

depth, $V_s^{(0)}$, and the transparency of the surface barrier for the electrons, $T_n$.

The general expression for the quantum yield, $Y$, obtained in the diffusion model for an arbitrary excitation intensity allows one to establish the dependence of the electron tunnelling probability through the surface barrier as a function of photovoltage using experimental data. The fitting to the experimental results of Ref. [51] gives the dependence $T_n(y) = {T_{n0}}^{(1+y)^\omega}$, where $y = \delta V/V_s^{(0)}$ $T_{n0}$ is the tunneling probability before illumination ($T_n = T_{n0}$ at y=0), and where the value of the power index, $\omega$, is $1/2 \div 3/4$. Such a dependence indicates that the surface barrier for the electrons is more triangular than rectangular and in atomic scale has a relatively low height. Thus the SCL phenomenon can be used for the characterization of the photocathode structure.

The SCL effect appears to be a limiting factor for emission current from strained-layer cathode structures, while the precise modulation doping that is possible in SL structures helps to reduce it [53]. To illustrate the SCL phenomenon in the SL cathodes, the response of the GaAs-AlGaAs SL structure with a moderate doping level of $N_a = 5 \times 10^{18}$ cm$^{-3}$ in an 11-nm-thick layer at the surface (after Ref. [53]) is presented in Fig. 10 for several values of the quantum yield, $Y$, of the SL at an excitation wavelength of 633 nm. The diminution of the $Y$ value is characteristic of the cathode temporal degradation and presumably originates from the decrease of the NEA. The limitation of the emitted charge is clearly seen for low quantum-efficiency surface states. However, a SCL is not observed at all for SL cathodes with a high doping level in the surface layer. For a doping level of $4\times10^{19}$ cm$^{-3}$, a multibunch beam with 1.6-A peak current, 12-ns bunch width, and 15-ns bunch separation has been produced that gives no evidence of the SCL phenomenon [53]. Most designs for future high-energy colliders require a multibunch structure that is more stringent, viz., a bunch width of about 1 ns with separation of 1–3 ns. Since a SL with a highly doped surface is a very promising candidate to be the polarized electron source for such colliders, measurements of the SCL using this type of cathode for generating the more demanding multibunch structure are anticipated in the near future.

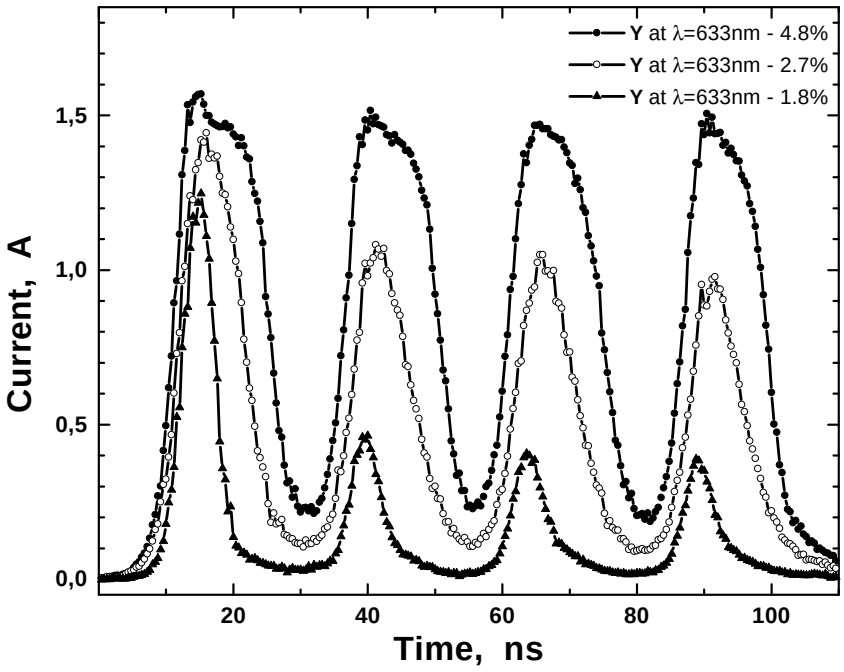


FIG. 10. Electron bunch shapes demonstrating charge saturation behaviours taken for different quantum yield states of a GaAs/AlGaAs superlattice with medium surface doping of $5 \times 10^{18}$ cm$^{-3}$ under quadruple-bunch laser excitation. Low-power values of $Y$ at 633-nm wavelength are shown in the picture. (Figure from Ref. [53].)

## III. APPLICATIONS

### A. Medium and High-Energy Physics

It has been nearly 25 years since polarized electrons were first accelerated to high energy in an electron accelerator. In the intervening period, polarized electron sources have evolved from relatively unwieldy experimental devices that were poorly matched to accelerator capabilities to highly reliable systems meeting all accelerator requirements for charge, stability, and reliability. A key element in this success has been the development of sources employing semiconductor photocathodes [55].

Accelerated beams of polarized electrons have proven to be powerful probes of the structure of the nucleon and also of the electroweak interaction. The techniques used to study

the structure of the nucleon include elastic electron-nucleon scattering and inelastic reactions induced by electrons. At medium energy ($Q^2 \ll M_Z^2$ where $M_Z$ is the mass of the $Z^0$ boson and $Q^2$ is the square of the 4-momentum of the virtual photon), the electromagnetic formfactors, $G_E(Q^2)$ and $G_M(Q^2)$, are measured in elastic electron-nucleon scattering experiments. For high $Q^2$ and even at low $Q^2$ for the neutron, $G_E$ is difficult to measure without polarized electrons. Nucleon resonance transitions can also be studied at medium energy. These measurements explore the interaction of quarks and gluons in confined systems. The use of polarized electrons for these experiments greatly expands the number of observables, which is crucial for distinguishing between competing models [56].

Measurement of the nucleon spin structure functions, $g_1(x, Q^2)$ and $g_2(x, Q^2)$, obtained from deep inelastic scattering of polarized electrons from polarized nucleon targets were actually the first accelerator-based experiments utilizing polarized electrons. Over the past few years these measurements have been extended to higher values of $Q^2$ and lower values of the fractional momentum of the parton, $\chi = Q^2/2M\nu$, where $M$ is the nucleon mass and $\nu$ is the electron energy transfer. The precision of this recent data has been made possible by the advent of the highly-polarized photocathodes now used in polarized electron sources. Pertubative QCD cannot predict an absolute value of $g_1$, however several relations have been derived that can be tested experimentally. Together with muon scattering data, the experimental results now confirm the validity of QCD while also pointing to a surprisingly low fraction of the total spin of the nucleon carried by quarks and indicating that the strange quarks are polarized opposite to the nucleon spin [57].

Polarized electron beams have also played an important role in the search for parity non-conservation (PNC). PNC arises from the interference of the electroweak and electromagnetic amplitudes. Left-right asymmetry measurements using polarized electron beams for which the helicity is randomly and frequently reversed are relatively free of systematic errors, and the results are subject to a straight-forward interpretation. The first such measurements using a polarized electron source with a GaAs photocathode provided an unambiguous measurement of PNC consistent with the predictions of the Standard Model (SM) [58].

Similar PNC measurements over a wide range of energies continue to be conducted at several accelerator laboratories with increasingly precise results. These experiments put extremely rigid requirements on the polarization and stability of the polarized electron sources.

A new era of polarized beam experiments began with the advent of the SLC polarized electron beam in 1992. The Stanford linear collider (SLC) and the CERN circular collider (LEP) were both designed to measure the properties of the $Z^0$ boson produced in $e^+e^-$ collisions at the $Z^0$ pole. The combined data from these experiments (now concluded) provide a measurement of the weak mixing angle, $\sin^2\ \theta_W^{\rm eff}$ , with a precision of $\approx$0.1 %. At LEP, four parallel experiments were conducted, the luminosity was extremely high, but neither beam was polarized. In the case of the SLC, its highly polarized (P$\approx$80%) electron beam was exploited to compensate for a relatively low luminosity and single experimental station. The power of a polarized beam for this type of experiment is illustrated by the fact that the precision of the combined SLC data is approximately the same as that of the combined LEP data although the latter included an order of magnitude more $Z^0$ events. In fact, of all the accelerator-based experiments, the left-right asymmetry measurement at the SLC using polarized electrons provides the single most precise determination of $\sin^2\ \theta_W^{\rm eff}$ [59].

Polarized electrons are expected to play an even more important role in future electron colliders. At collision energies of $\approx$500 GeV in the center of mass, the cross sections for many processes depend on polarization. A particularly striking example is that the production of $W^+W^-$ pairs, which provide a major part of the background for many other processes, is nearly suppressed for a right-handed electron beam. Within supersymmetry (SUSY), the production of right-handed sleptons and neutralinos dominates for a right-handed beam, whereas left-handed sleptons and charginos dominate for left-handed [60]. Thus polarization will be very useful for sorting out SUSY signals. In addition, precision measurements of properties of SUSY particles will benefit from the background reduction available with right-handed electron beams. In the rather dramatic example shown in Figure 11, the dominating $W^+W^-$ background associated with smuon pair production using an unpolarized electron

beam is nearly eliminated by using a highly polarized beam. Finally, as will be discussed below, polarized beams enhance the luminosity of a collider.

The principal reason for the effectiveness of polarized electrons for energies $> M_Z$ is that right-handed electrons, $e_R^-$ , have no weak interaction whereas left-handed electrons, $e_L^-$, do. Consequently, above the $Z^0$ mass, $e_R^-$ and $e_L^-$ behave as distinctly different particles.

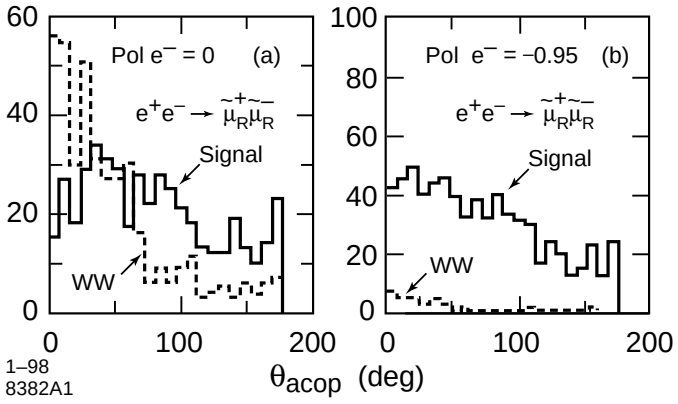


FIG. 11. Examples of acoplanarity distributions for smuon pair production with (a) unpolarized electron beam, and (b) a 95 % right-hand polarized beam. (Figure from Ref. [61]).

Wherever cross sections have a strong dependence on polarization, about half the particles in an unpolarized beam are useless. By choosing only the desired particles for an interaction, the luminosity for a given beam intensity is effectively increased.

For future lepton colliders, the electron beam polarization of ≈80 % that is already available will be sufficient for most high-energy physics experiments. A possible exception may be for the study of charginos since their cross sections vary with the handedness of the beam polarization in nearly the same manner as the $W^+W^-$ background. However, there is no question but that having significantly higher polarization will have an enormous impact on the physics capabilities of a future collider.

### B. Magnetic properties of materials

In solid-state physics and in the physics of semiconductors, spin-polarized electron spectroscopies are powerful tools for the study of surface and thin-film magnetism and of the electronic structure of metal and semiconductor surfaces and films [5]. Advances in information technology require corresponding increases in storage density on magnetic media, leading to a reduced bit-size of weak signal-strength. Therefore surface and interface effects will soon dominate the magnetic properties of new storage media. This perspective has made thin magnetic films one of the most promising research topics in applied science, which - within only 10 years - has lead from the discovery of interlayer coupling to the production of GMR-Write/Read Heads [62] and to the development of magneto-optical media and magneto-resistive "random access memory". Yet further basic research is necessary to gain an understanding of magnetic anisotropy and various other phenomena which restrict the present performance of thin-film devices. Here spin-resolved techniques such as photoemission (PE), inverse photoemission (IPE), and appearance potential spectroscopy (APS) are the proper methods to study the electronic band structure near the Fermi level ($E_F$), which is the "driving force" behind magnetic coupling strength, coercivity, and other technical parameters. The information depth for low-energy electrons is determined by the electron inelastic mean free path in the sample. A linear relationship between the inverse mean free path and the number of the empty *d*-states was found to describe (see Ref. [5]) the data of a variety of materials well. This proves the relevance of empty *d*-states as final states for inelastic scattering processes. The information depth for low-energy electrons in ferromagnetic 3d-materials is about 2 to 3 monolayers only. This feature makes spin-resolved low energy electron spectroscopies of great importance for surface and thin-film studies.

In the case of appearance potential spectroscopy (APS), which is an inverse Auger electron spectroscopy, the solid is bombarded with electrons of variable energy while the total yield of emitted X-rays or electrons is monitored. At energies high enough (appearance potential) to excite a core electron into empty states above $E_F$, the yield of emitted par-

ticles increases due to recombination of the created core hole via X-ray or Auger-electron emission. Since both the excited and the exciting electron are scattered into empty states, the rate of possible excitations and, thereby, of detected recombinations depends on the density of states above $E_F$. The elemental resolution comes from the fact that core levels are involved whose energies are characteristic of the different elements. The use of spin-polarized electrons makes APS magnetically sensitive because the number of empty states in a ferromagnet depends strongly on the spin direction relative to the quantization axis of the system given by the magnetization direction [63]. Applied to an ultrathin film system, spin-resolved APS provides combined information about structural and magnetic properties [64].

Angle-resolved inverse photoemission spectroscopy (IPE) [65,66]) allows one to obtain information about the unoccupied electronic states above the Fermi level, complementary to ultraviolet photoelectron spectroscopy that yields information on the occupied band structure. The basis of IPE is as follows: an incident low energy electron enters the solid and undergoes an electronic transition from a higher-lying level to a lower level, emitting a photon. The number of photons at a given photon energy as a function of the incident kinetic energy is a measure of the joint density of unoccupied states. As in angle-resolved ultraviolet PE, band mapping is done by varying the angle of incidence. Spin-polarized IPE (SPIPE) is sensitive to the spin-splitted features of the surface band structure and, hence, to the magnetic properties of the surface [67].

Spin resolved IPE data from Fe(001) and Fe(001)-$p(1\times1)$O surfaces are collected in Fig. 12 showing the IPE spectra for majority- and minority-spin electrons [68]. Three features are seen in the spectra, labeled as $B_1$, $B_2$ and $S$. In Fe(001) $B_1$ and $B_2$ correspond to bulk transitions towards majority- and minority-spin empty states near the $H$ point of the bcc Brillouin zone ($H'_{25}$ levels). The feature $S$ originates from transitions into the image state resonance, which in Fe(001) presents an unusual inversion of the majority- and minority-spin levels. In Fe(001)-$p(1\times1)$O the bulk derived structures are attenuated, while a new and completely polarized O induced peak, overlapping $B_2$, appears. An image state peak is

also visible at the same energy as in the clean surface. The energy of such a state is indeed bound to $E_V$, which does not change upon oxidation.

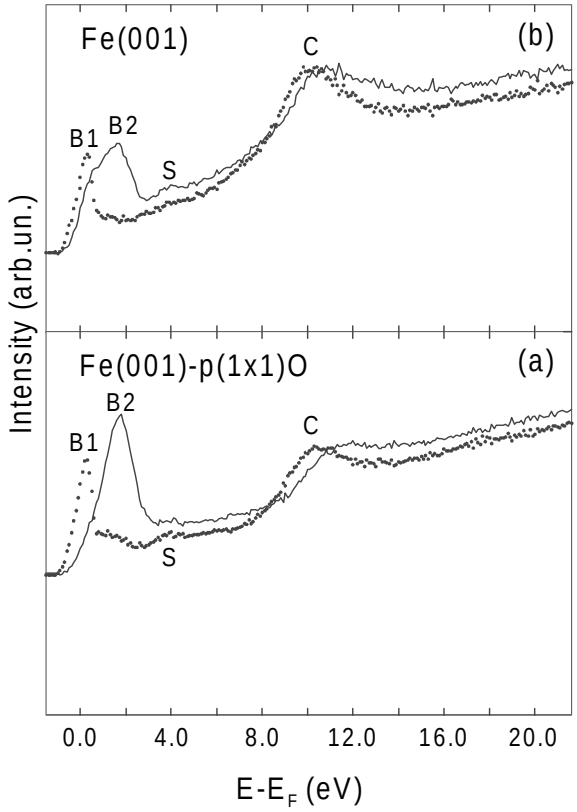


FIG. 12. Spin resolved IPE spectra for the Fe(001)-$p(1\times1)$O and Fe(001) surfaces. The data are normalized to a hypotethical 100% incident beam polarization through a standard procedure . (Figure from Ref. [68]).

Until now IPE has been the main method that gives detailed information on the unoccupied band structure of crystalline magnets. The measurement time of SPIPE is today limited by the "standard" (GaAs) photocathode, which has a maximum polarization of about $P$=30 %. The time (scaling with $1/P^2$) could easily be reduced by an order of magnitude by using more efficient cathodes that give $P$ of about 80% or more. But it is not only time saving which makes these cathodes desirable. Due to the higher polarization degree, the measured signal would become more reliable, giving one the opportunity to tackle key questions in magnetism which have so far been out of reach: what is the crucial ingredient for perpendicular magnetization in the spin dependent electronic structure? What is the degree of

correlation between the d-electrons in a typical magnetic multilayer? To face these questions, a FU Berlin - SPTU - VICS Ltd. (St. Petersburg) collaboration is planning to build a new highly efficient polarized electron source (PES) with variable spin direction ("spin-flipper"). Such a source, together with a compact spin-detector, will give access to the band structure of technologically important films showing a 'spin-reorientation' from in-plane to out-of-plane magnetisation. This system should be helpful as well for a recently proposed technique to study magnetic materials [69]: spin- and - angle resolved energy correlated coincidence electron spectroscopy of solid surfaces.

## IV. CONCLUSIONS

In the last decade the physics of spin-polarized electrons in semiconductors has proven to be not only a fascinating field for fundamental study but also a fruitful field for device applications that have had a significant impact in several fields of modern physics. The history of the development of highly polarized electron sources is short but spectacular. Progress in semiconductor technology and, particularly, in the growth of highly stressed heterostuctures and short-period superlattices was decisive for this success.

From a more general point of view, the productivity of the "band structure engineering" concept is clearly manifest. The most probable prediction of the future evolution of this field is toward the development of new and more complex heterostuctures with optimally chosen parameters. Modern trends in the semiconductor physics have broaden the range of prospective structures to include systems of ordered quantum wires and quantum dots, which augurs well for the next decade of polarized electron source research.

An important problem for future investigation, among others, concerns the quest for a more predictable and manageable activation procedure that can be used to reliably lower the crystal work function. Progress in this field will result presumably from deeper experimental and theoretical studies of disorder effects in the strongly interacting two-dimensional Coulomb system in the band-bending region of the activated semiconductor surface as well

as from progress in the investigation of the atomic structure of the activation layers.

## Acknowledegments

This work is supported by the Russian State Program "Surface atomic structures", project No. 95-1.23 and the U.S. Civilian Research and Development Foundation under Award No. RP1-351. Support by the Russian Foundation for Basic Research, project No. 96-02-19187 is also gratefully acknowledged. One of us (J.E. Clendenin) is supported by the U.S. Department of Energy, contract DE-AC03-76SF00515. The authors are thankful to Prof. T. Nakanishi and Dr. K. Togawa (Nagoya University, Japan), Prof. F. Ciccacci (Politechnico di Milano, Italy) and Dr. J. Schuler (Mainz University, Germany) for placing their results at our disposal and Dr.K. Starke and Dr. S. Bode (Free University, Berlin) for fruitful discussion.

# REFERENCES


[1] T.Maruyama, E.L.Garvin, R.Prepost et al., Phys. Rev. Lett., 66 (1991) 2376.

[2] T.Nakanishi, H.Aoyagi, H.Horinaka et al., Phys. Lett., A 158 (1991) 345; T.Maruyama, E.L.Garvin, R.Prepost et al., Phys. Rev., B 46 (1992) 4261.

[3] *Proc. of the Workshop on Photocathodes for Polarized Sources for the Accelerators*, SLAC, 1993, edited by M.Chatwell et al., SLAC-Report-432 Rev., 1994.

[4] D.T.Pierce, in *Experimental Methods in Atomic, Molecular and Optical Physics: Charged Particles*, edited by F.B.Dunning and R.G.Hulet, v. 29A of the series Experimental Methods in the Physical Sciences, Academic Press, 1995, p. 1.

[5] H.C.Siegmann, J. Phys.:Cond. Matt., 4 (1992) 8395.

[6] *Optical orientation,* edited by F.Meier and B.P.Zakharchenya, North-Holland, 1984.

[7] R.L. Bell, *Negative Electron Affinity Devices*, Oxford Univ. Press, 1973.

[8] G.Pikus and G.Bir, *Symmetry and strain induced effects in semiconductors*, Wiley, 1974.

[9] Yu.A.Mamaev, Yu.P.Yashin, A.V.Subashiev, at al., Phys. Low Dim. Struct., 7 (1994) 27.

[10] Yu.P.Yashin, Yu.A.Mamaev and A.N.Ambrazhei, *Proc. of the Low Energy Polarized Electron Workshop* LE-98, St.-Petersburg, 1998, edited by Yu.A.Mamaev et al., SPES-Lab-Pub., 1998, p. 27.

[11] W.Spicer, Phys. Rev. 112 (1958) 114; J. Appl. Phys., 31 (1960) 2077.

[12] A.S.Terekhov and D.A.Orlov, JETP Lett., 59 (1994) 864; also Proc. SPIE, 2550 (1995) 157.

[13] B.D.Oskotskij, A.V.Subashiev, and Yu.A.Mamaev, Phys. Low Dim. Struct., 1/2 (1997) 77.

[14] A.V.Subashiev and E.P.German, in *Polarized Gas Targets and Polarized Beams, 7-th Intern. Workshop*, Urbana, 1997, edited by R.Holt et al., AIP Conf. Proc. 421, 1998, p. 489.

[15] A.V.Subashiev and E.P.German, JETP Lett., 65 (1997) 909.

[16] R.Mair, SLAC-Report-488, 1996; T.Maruyama et al., *Proc. of the Low Energy Polarized Electron Workshop* LE-98, St.-Petersburg, 1998, edited by Yu.A.Mamaev et al., SPES-Lab-Pub., 1998, p. 13.

[17] H.Aoyagi, H.Horinaka, Y.Kamiya et al., Phys. Lett., A 167 (1992) 415.

[18] J.-C.Gröbli et al., Phys. Rev. Lett., 74 (1995) 2106.

[19] R.Mair, R.Prepost, H.Tang et al., Phys. Lett., A 212 (1996) 231.

[20] J.E.Clendenin, Int. J. Mod. Phys., A 13 (1998) 2507.

[21] T.Omori, Y.Kurichara, Y. Takeushi, et al., Jpn. Journ. Appl. Phys., 33 (1994) 5676.

[22] T.Nakanishi, S.Okumi, M.Tavada et al., in *Proc. of 12th International Symposium on High-Energy Spin Physics*, Amsterdam, 1996, edited by C.W.D. de Jager et al., World Scientific, 1997, p. 712.

[23] Yu.A.Mamaev, A.V.Subashiev, Yu.P.Yashin, at al., Phys. Low Dim. Struct., 10/11 (1995) 61.

[24] T.Nakanishi, S.Okumi, K.Togawa at al., in *Polarized Gas Targets and Polarized Beams, 7-th Intern. Workshop*, Urbana, 1997, edited by R.Holt et al., AIP Conf. Proc. 421, 1997, p. 300.

[25] I.A.Merkulov, V.I.Perel' and M.E.Portnoy, Sov. Phys.-JETP, 72 (1991) 669.

[26] L.G.Gerchikov, G.V.Rozhnov and A.V.Subashiev, Sov. Phys.-JETP, 74 (1992) 77.

[27] A.V.Subashiev, in *Proc. of 12th International Symposium on High-Energy Spin Physics*,

Amsterdam, 1996, edited by C.W.D. de Jager et al., World Scientific, 1997, p. 749.

[28] G.Arnaud, P.Boring et al., Phys. Rev., B 46 (1992) 1886 .

[29] E.L.Ivchenko, P.S.Kop'ev, V.P.Kochereshko et. al., JETP Lett., 47 (1988) 486.

[30] A.V.Subashiev, Yu.A.Mamaev, Yu.P.Yashin, J.E.Clendenin et al., SLAC-Pub-7922, Aug. 1998, to be published in Proc. Intern. Conf. on Phys. of Semicond. (ICPS-24), Jerusalem, 1998.

[31] G.E.Pikus and A.N.Titkov, in *Optical orientation* edited by F.Meier and B.P.Zakharchenya, North-Holland, 1984, p. 73.

[32] G.E.Pikus, V.A.Maruschak and A.N.Titkov, Sov.Phys.-Semicond., 22 (1988) 160.

[33] M.C.P.Krijn, Semicond. Sci. Technol., 6 (1991) 27.

[34] A.V.Subashiev,Yu.A.Mamaev, Yu.P.Yashin, J.E.Clendenin et al., SLAC-Pub-7995, Nov. 1998; *Proc. of the Low Energy Polarized Electron Workshop* LE-98, St.-Petersburg, 1998, edited by Yu.A.Mamaev et al., SPES-Lab-Pub., 1998, p. 55

[35] C.Herman, H.-J.Drouhin, G.Lampel et al., in *Spectroscopy of Nonequilibrium Electrons and Phonons*, edited by C.V.Shank and B.P.Zakharchenya, Elseiver Science B.V., 1992, p. 397.

[36] S.Pastuszka, D.Kratzmann, D.Schvalm et al., Apl. Phys. Lett., 71 (1997) 2967.

[37] V.E.Andreev, V.V.Bakin, D.A.Orlov et al., *Proc. of the Low Energy Polarized Electron Workshop* LE-98, St.-Petersburg, 1998, edited by Yu.A.Mamaev et al., SPES-Lab-Pub., 1998, p. 163.

[38] H.Tang et al. In *Proc. of the Workshop on Photocathodes for Polarized Electron Sources for Accelerators*, SLAC, 1993, SLAC–Report-433 Rev., 1994, p. 344.

[39] H.-J.Drouhin, C.Herman and G.Lampel, Phys. Rev. B 31 (1985) 3859; *ibid.* 31 (1985)

3872.

[40] H.Riechert, S.F.Alvarado, A.N.Titkov and V.I.Safarov, Phys. Rev. Lett., 52 (1984) 2297.

[41] R.G.Ulbrich, J.A.Kash and J.C.Tang, Phys. Rev. Lett., 62 (1989) 949.

[42] L.G.Gerchikov, B.D.Oskotskij and A.V.Subashiev, in *Proc. of 12th International Symposium on High-Energy Spin Physics*, Amsterdam, 1996, edited by C.W.D. de Jager et al., World Scientific, 1997, p. 746.

[43] B.D.Oskotskij, A.V.Subashiev, and L.G.Gerchikov, in *Polarized Gas Targets and Polarized Beams, 7-th Intern. Workshop*, Urbana, 1997, edited by R. Holt et al., AIP Conf. Proc. 421, 1998, p. 491.

[44] For more detailed discussion of the effects of the charge density fluctuations in the BBR on the density of states and the ME see e.g. V.A.Gergel' and R.A.Suris, Sov.Phys.-JETP, 57 (1983) 415, and M.S.Bello, E.I.Levin, B.I.Schklowskii and A.L.Efros, Zh. Exp. & Teor. Fiz., 80 (1981) 1596.

[45] A.V.Subashiev, *Proc. of the Low Energy Polarized Electron Workshop* LE-98, St.-Petersburg, 1998, edited by Yu.A.Mamaev et al., SPES-Lab-Pub., 1998, p. 125.

[46] Analogous arguments are used in the discussion of the luminescence spectra of disordered solid solutions and amorphous solids, see e.g. A.G.Abdukadyrov, S.D.Baranovskii, S.Yu.Verbin et al., Sov.Phys-JETP, 71 (1990) 1155.

[47] J. Schuler, K. Aulenbacher, T. Baba et al., *Proc. of the Low Energy Polarized Electron Workshop* LE-98, St.-Petersburg, 1998, edited by Yu.A.Mamaev et al., SPES-Lab-Pub., 1998, p. 20.

[48] M.Woods et al. J. Appl Phys., 73 (1993) 8531.

[49] H.Tang, R.K.Alley, H.Aoyagi et al., in *Fourth European Particle Accelerator Conference*, London, 1994, World Scientific, 1994, p. 46.

[50] Y.B.Bolkovityaninov et al., in *Proc. of 12th International Symposium on High-Energy Spin Physics*, Amsterdam, 1996, edited by C.W.D. de Jager et al., World Scientific, 1997, p. 700.

[51] A.S.Jaroshevich et al., in *Polarized Gas Targets and Polarized Beams, 7-th Intern. Workshop*, Urbana, 1997, edited by R.Holt et al., AIP Conf. Proc. 421, 1998, p. 485.

[52] A.Herrera-Gómez, G.Vergara and W.E.Spicer, J. Appl. Phys., 79 (1996) 7318.

[53] K.Togawa, T.Nakanishi, T. Baba et al., Nucl. Instrum. and Meth., A 414 (1998) 431; also *Proc. of the Low Energy Polarized Electron Workshop* LE-98, St.-Petersburg, 1998, edited by Yu.A.Mamaev et al., SPES-Lab-Pub., 1998, p. 133.

[54] B.I.Reznikov and A.V.Subashiev, Sov.Phys.-Semicond., 32 (1998) 1005; *ibid.* 32 (1998) 1352.

[55] R.Alley et al., Nucl. Instrum. and Meth., A 365 (1995) 1.

[56] V.Burkert, in *Proc. of 7th International Conference on Polarization Phenomena in Nuclear Physics*, Paris, 1990, Colloq. Phys. C (1990) p. 283.

[57] G.K.Mallot, in *Proc. of 12th International Symposium on High-Energy Spin Physics*, Amsterdam, 1996, edited by C.W.D. de Jager et al., World Scientific, 1997, p. 44.

[58] C.Y.Prescott et al., Phys. Lett., 77B (1978) 347.

[59] P.B.Renton, Oxford University preprint OUNP-98-04 (1998).

[60] M.Danielson et al., in *New Directions for High-Energy Physics*, Proc. of the 1996 DPF/DPB Summer Study on High-Energy Physics, Snowmass, 1996, edited by D.G. Cassel et al., SLAC, 1997, p. 720.

[61] K.Fujii, in *Workshop on Physics and Experiments with Linear Colliders*, Morioka-Appi, Iwate, 1995, edited by A.Miyamoto et al., World Scientific, 1996, p. 283.

[62] P.Gruenberg et al., Phys. Rev. Lett., 57 (1986) 2442; IBM purchased the patent in 1995.

[63] J.Kirschner, Solid State Comm., 49 (1984) 39.

[64] Th.Detzel et al., Phys. Low-Dim. Struct., 8/9 (1995) 1.

[65] J.Unguris et al., Phys. Rev. Lett.,49 (1982) 1047.

[66] M.Donath, Surf. Sci. Rep., 20 (1994) 251.

[67] S.Bode, K.Starke and G.Kaindl, J. Magn., 148 (1995) 183.

[68] S.De Rossi, L.Duo and F.Ciccacci, Europhys. Lett., 32 (1995) 687; S.De Rossi and F.Ciccacci, J. Electr. Spectr. Relat. Phenom., 76 (1995) 177.

[69] J.Berakdar et al., Phys. Rev. Lett., 81 (1998) 3535.